




Ultrafast optical generation of antiferromagnetic meron-antimeron pairs with conservation of topological charge

Sumit Ghosh ^{1,2,*}, Stefan Blügel ¹ and Yuriy Mokrousov ^{1,2}

¹*Peter Grünberg Institut (PGI-1), Forschungszentrum Jülich GmbH, 52428 Jülich, Germany*

²*Institute of Physics, Johannes Gutenberg-University Mainz, 55128 Mainz, Germany*

 (Received 8 December 2022; revised 21 February 2023; accepted 17 March 2023; published 7 April 2023)

We propose a new mechanism to produce a meron-antimeron pair in a two dimensional antiferromagnet with an ultrafast laser pulse via a thermal Schwinger mechanism. Unlike ultrafast skyrmion nucleation, this process conserves total topological charge. We systematically show different stages of the dynamics and define proper topological invariants to characterize the configurations. The emergent structure can retain its topological structure for up to 100 ps. By introducing a topological structure factor we show that pair formation is robust against any random choice of initial magnetic configuration and can survive against disorder. Our findings demonstrate that the rich world of spin textures, which goes beyond conventional skyrmions, can be reached optically.

DOI: [10.1103/PhysRevResearch.5.L022007](https://doi.org/10.1103/PhysRevResearch.5.L022007)

I. INTRODUCTION

In the quest for a fast and efficient mechanism for manipulating magnetic order, ultrafast optical manipulation of magnetism emerged as one of the most promising paradigms. Interaction between an ultrafast laser and magnetic moments takes place at a much faster timescale and consumes far less energy [1,2] compared to electrical switching [3]. The underlying physical mechanism is, however, still in a mist. From the initial experimental demonstration of ultrafast demagnetization [4], this effect was considered to be of thermal origin conventionally modeled with the phenomenological three temperature model. Zhang and Hübner [5] proposed a microscopic mechanism mediated by spin-orbit coupling, whereas Koopmans and co-workers proposed an alternative mechanism mediated by electron-phonon coupling [6]. These theoretical frameworks aim to understand the transition from ordered magnetic states to strongly disordered and often non-magnetic states, which gives the impression that the governing mechanism behind the ultrafast demagnetization is of thermal origin [7]. Based on time-dependent density functional theory approach, Dewhurst *et al.* recently proposed an alternative mechanism [8] for transferring angular momentum between different sites, which has been subsequently observed experimentally [9]. This mechanism relies on a coherent redistribution of spin angular momentum [10] and therefore can be exploited to drive a ferromagnet-to-antiferromagnet transition [11].

In this context, an ability to generate any desired magnetic configuration, i.e., a spin texture of desired properties with an ultrafast optical laser, remains a challenge. Recent experimental demonstration of skyrmion nucleation with an ultrafast laser by Büttner *et al.* [12] has proved the feasibility of optical generation of spin textures. However, the proposed explanation of the effect relies solely on classical magnetization dynamics which does not take into account electronic interactions. Besides, the working model contains the antisymmetric Dzyaloshinskii-Moriya interaction which is known to drive the system into a skyrmionic state without any additional excitation [13]. The nucleation process can be further reinforced with a laser [14] in the presence of spin-orbit coupling. Such topological structures are also known to arise during the transition between two different magnetic configurations [15,16]; however, their transient nature makes them useless for any practical purpose. An alternative mechanism of laser induced magnetization dynamics was recently proposed by Ghosh and co-workers [17], showing the emergence of a new chiral spin-mixing interaction which can lead to chiral formation even in absence of any intrinsic spin-orbit coupling. The emergent chirality is quite sensitive to the laser parameters which emphasizes the importance of coherent interaction of the laser with the electronic degrees of freedom for chiral state generation. This mechanism leads to a quasistable chiral formation which can survive for several picoseconds, and it is distinctly different from that driven by thermal excitations.

It is well-known that skyrmions are nontrivial magnetic configurations that are equivalent to magnetic monopoles which can be characterized by a skyrmion number [18]. To understand the dynamics of the skyrmions or similar quasiparticles, one can look into the physics of monopoles from the perspective of field theory [19]. Due to their heavy mass [20,21], creating isolated magnetic monopoles still remains quite challenging. An alternative paradigm would lie in producing a monopole-antimonopole pair [22], which is also

*s.ghosh@fz-juelich.de

Published by the American Physical Society under the terms of the [Creative Commons Attribution 4.0 International license](https://creativecommons.org/licenses/by/4.0/). Further distribution of this work must maintain attribution to the author(s) and the published article's title, journal citation, and DOI.

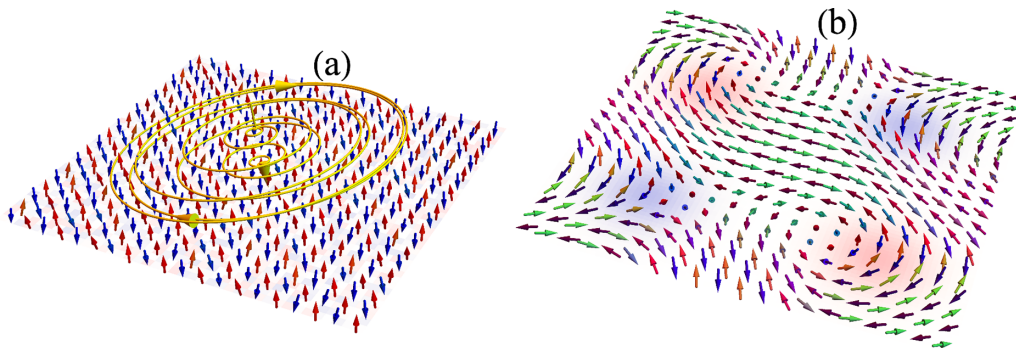


FIG. 1. Generation of a meron-antimeron pair by an ultrafast laser pulse. (a) Initial antiferromagnetic configuration. Yellow line denotes the circularly polarized laser. (b) Emergence of a quasistable meron-antimeron pair after the action of the laser pulse. The blue and red regions show the negative and positive topological charge.

making its appearance in recent experimental observations of magnetic textures. Indeed, topological spin textures often emerge in pairs consisting of a texture and its antitexture, keeping the total topological charge to zero. Such pair formation has been observed both at metallic interfaces [23] and predicted in two-dimensional magnets [24,25]. These pairs can be further transmuted to a pair of different but opposite textures (for example meron to skyrmion [26] conversion by an external magnetic field) without violating the conservation of topological charge.

All these studies so far have been done on ferromagnetic materials which naturally raises an alluring question—is it possible to combine the aforementioned ideas and stimulate such pair production in an antiferromagnet via an optical excitation? Antiferromagnets are favorable materials due to their natural abundance and faster response as compared to ferromagnets. Besides, they are immune to any external magnetic field and also demonstrate rich and topologically nontrivial electronic properties. However, regarding the nontrivial real space textures in antiferromagnets, reported studies are restricted to a narrow domain of skyrmions only [27]. Here, we demonstrate that it is indeed possible to go beyond skyrmions and nucleate meron-antimeron pairs in an antiferromagnet with an ultrafast laser pulse (Fig. 1). We present a systematic study of the different stages of nucleation and demonstrate the gradual formation of meron-antimeron pair starting from a collinear antiferromagnetic state. We analyze different physical observables at different stages of the dynamics and define a proper topological invariant to characterize their dynamical evolution. Finally, we reveal the robustness of the overall process versus disorder.

II. MODEL AND METHOD

We define a two-dimensional antiferromagnet on a square lattice with a time dependent double-exchange Hamiltonian [17,28,29]

$$H(t) = -J \sum_{i;\mu,\nu} c_{i,\mu}^\dagger (\hat{\mathbf{m}}_i \cdot \boldsymbol{\sigma})_{\mu\nu} c_{j,\nu} - \sum_{i,j;\mu} h_{ij}(t) c_{i,\mu}^\dagger c_{j,\nu}, \quad (1)$$

where $c_{i,\mu}^\dagger, c_{i,\mu}$ are the creation (annihilation) operators of an electron at site i with spin μ . $\hat{\mathbf{m}}_i$ is a unit vector at site i denoting the direction of the magnetization and $\boldsymbol{\sigma}$ is

the vector of Pauli spin matrices. J denotes the coupling between the local magnetic moment and the itinerant moment which, following Hund's rule, is kept positive [29] and set to 1 eV. $h_{ij}(t)$ is the time-dependent hopping parameter between site i and site j . The action of the laser is defined as a time varying electric field with a Gaussian envelope modeled as a time varying vector potential $\mathbf{A}(t) = -\frac{\mathcal{E}_0}{\omega} e^{-(t-t_0)^2/2s^2} (\cos(\omega(t-t_0))\hat{\mathbf{x}} + \sin(\omega(t-t_0))\hat{\mathbf{y}})$, where \mathcal{E}_0 is the peak amplitude of laser occurring at time $t = t_0$, and ω is the angular frequency. s denotes the broadening of the pulse which we kept at 5 fs. In this work we keep $\mathcal{E}_0 = 0.1 \text{ eV } a_0^{-1}$ (a_0 being the lattice constant), and $\omega = 2.02 |J|/\hbar = 3.07 \times 10^{15} \text{ Hz}$. The frequency is chosen such that the laser connects the unoccupied states with the occupied states which are separated by an energy gap of $2|J|$. The action of the laser is incorporated in the Hamiltonian [Eq. (1)] via Pierel's substitution $h_{ij}(t) = h e^{i(e/\hbar)\mathbf{A}(t)\cdot\mathbf{r}_{ij}}$, where \mathbf{r}_{ij} is the vector connecting site i to site j . The static value of the hopping parameter is kept at $h = 0.4 \text{ eV}$. The qualitative behavior of the system remains consistent within a moderate range of these parameters [17]. For our study we consider a supercell of dimension 20×20 with periodic boundary condition.

The ground state is constructed by filling half of the lowest eigenvalue states which, in our case, are all the states with negative eigenvalues. For our choice of parameters, this corresponds to an antiferromagnetic alignment [17,28]. We simulate the thermal equilibrium at finite temperature by adding a small random fluctuation (0.1π) to the polar angles while the azimuthal angles are chosen randomly between 0 and 2π . This randomness is crucial to initiate the magnetization dynamics by generating initial spin-mixing interaction [17]. Note that our initial configuration does not possess any spin-orbit coupling or any specific noncollinear order and therefore constitutes a trivial antiferromagnetic insulator. At any instance of time t , any quantum state $|\psi_t\rangle$ can be expressed as the linear combination of instantaneous eigenstates $|n(t)\rangle$ of the Hamiltonian which is evolved within a Schrödinger picture [17,28]. This allows us to evaluate the instantaneous effective field for any site i as $\frac{1}{\mu_B} \sum \langle \psi_t | -\nabla_{\mathbf{m}_i} H | \psi_t \rangle$, μ_B being the Bohr magneton. This effective field is used in a set of Landau-Lifshitz-Gilbert equations [17,29,30]

$$\frac{d\mathbf{m}_i}{dt} = -\gamma(\mathbf{m}_i \times \mathbf{B}_i) - \lambda \mathbf{m}_i \times (\mathbf{m}_i \times \mathbf{B}_i), \quad (2)$$

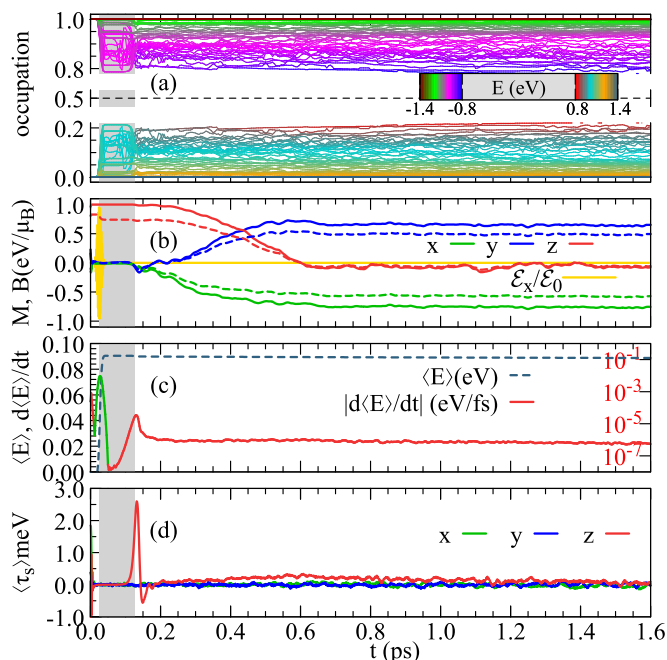


FIG. 2. Time evolution of different physical observables. (a) Change of occupation for different states with their color denoting corresponding eigenvalues. Here we show every 5th state. Gray shaded region shows the time delay between the incident of laser and onset of magnetization dynamics. (b) Change of magnetization vector (solid) and effective field (dashed) components of the magnetic moment at $x = 1, y = 10$. Yellow line denotes the x component of the laser electric field. (c) Change of average total energy (gray dashed) and rate of change of energy (red) where the green portion shows when the system absorbs energy. (d) Evolution of different components of average torque.

where $\gamma = \frac{g_e \mu_B}{\hbar \mu_s} \frac{1}{1+\alpha^2}$, $\lambda = \frac{g_e \mu_B}{\hbar \mu_s} \frac{\alpha}{1+\alpha^2}$, where g_e is the gyromagnetic ratio, μ_s is the onsite magnetic moment which we keep at $1 \mu_B$ and α is the dimensionless damping coefficient, which we keep fixed at 0.2. $\mathbf{m}_i \times \mathbf{B}_i$, constitutes the local torque. One can add an additional stochastic torque [31] to simulate thermal fluctuation. For simplicity we neglect such a thermal effect since the topological nature of the outcome remains robust at low temperature.

III. RESULT AND DISCUSSION

After the action of the ultrafast laser, one can observe three different phases of dynamics originated from complex interactions between electronic and magnetic degrees of freedom (Fig. 2). The peak amplitude of the laser occurs at $t = 25$ fs [Fig. 2(b)], marked by the left edge of the gray area in Fig. 2. This triggers a redistribution of occupation of quantum states [Fig. 2(a)] which in turn start building the torque. An initial randomness is imperative to start this process which also determines how fast the system can respond to the pulse [17]. In our present setup, after a latency period of approximately 100 fs (right edge of gray region in Fig. 2), the magnetic moments start reorganizing themselves causing the fast relaxation phase [17] that lasts for approximately 0.5 ps [Fig. 2(b)]. The system then enters into the slow relaxation phase which

eventually leads to the final texture shown in Fig. 1. Note that the energy absorption takes place only during the short duration defined by the Gaussian envelope of the pulse [green segment in Fig. 2(c)]. The steady state can be characterized by evaluating the average staggered torque [32] defined as $\langle \tau_s \rangle = 1/N \sum_{ij} v_{ij} (\mathbf{m}_{ij} \times \mathbf{B}_{ij})$, where the index i, j corresponds to the position, $v_{ij} = \pm 1$ is the sublattice index, and N is the total number of sites. Note that the optical excitation predominantly produces the out of plane component of the torque [Fig. 2(d)] leading to the final in-plane texture. Assuming that the average energy gain per site is ~ 0.1 eV with the dissipation rate being 10^{-6} eV fs $^{-1}$, it would take the system about 100 ps to dissipate the excess energy and regain its initial configuration. It is worth mentioning that due to the complex intertwined electronic and magnetization dynamics, the energy dissipation of the system is not solely determined by the phenomenological damping parameter only and additional dissipation channels can emerge during different stages of the dynamics. This can be verified from the energy dissipation rate of the system at steady state which is found to decrease with the increase of damping parameters for such laser excited systems [17].

A. Dynamical evolution of topological charge

From Fig. 1, one can see that the final configuration contains a pair of antiferromagnetic meron and antimeron. This is reminiscent of a Schwinger mechanism which produces a particle and antiparticle. Similar mechanisms can also generate monopole-antimonopole pairs [33] that can survive even in the presence of a thermal bath [34]. Such pair nucleation for topological defects was also predicted in the context of bubble collision [35] following a Kibble mechanism [36]. To characterize the pairs we choose their skyrmionic charge. On a ferromagnetic background, each meron can be characterized by a skyrmion number $\pm \frac{1}{2}$, resulting in a total zero skyrmion number for the whole configuration. For an antiferromagnet, one can define a skyrmion number for each sublattice [16], however, it does not take the intersublattice interaction properly into account. To avoid this, we define a staggered skyrmionic charge (Fig. 3)

$$S_{ij}^s = v_{ij} [\mathbf{m}_{ij} \cdot (\partial_x \mathbf{m}_{ij} \times \partial_y \mathbf{m}_{ij})], \quad (3)$$

where $v_{ij} = \pm 1$ for the opposite sublattices and $\partial_x \mathbf{m}_{ij} = (\mathbf{m}_{i+1,j} - \mathbf{m}_{i,j})$. Since the total skyrmionic charge of the complete cell is zero, we use an absolute skyrmion density $S_{\text{Tot}}^s = \sum |S_{ij}^s|$ to characterize the configuration. For a well-isolated meron-antimeron pair, this number should be one. However, due to the finite size there is always some overlap between the different regions causing a deviation of the total absolute skyrmion charge from two for the whole supercell [Fig. 3(b)]. For a proper topological characterization in this case, we evaluate the winding number [37] for all four meron/antimeron centers defined as

$$\mathcal{W} = \frac{\mathcal{P}_s}{2\pi} \oint_{\mathcal{C}} d\mathbf{l} \cdot \nabla \phi, \quad (4)$$

where \mathcal{P}_s is the sublattice polarization, given by $\text{sgn}(m_z) \cdot \nu$ with m_z being the out of plane component of the magnetization at the center and $\nu = \pm 1$ for the sublattices. ϕ is the azimuthal angle and the contour \mathcal{C} encircles the winding

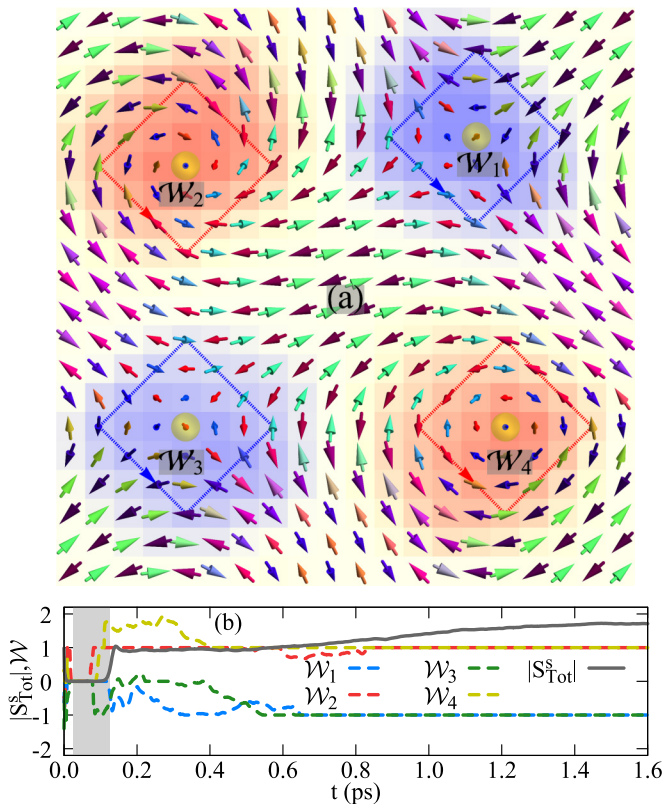


FIG. 3. Skymionic charge and winding number for antiferromagnetic meron-antimeron pairs. (a) Distribution of skymionic charge is shown with red and blue color denoting positive and negative values, with winding centers $W_{1,2,3,4}$ marked with yellow spheres. Solid blue and red lines show the contours along which winding number is calculated with red and blue colors denoting a winding number ± 1 . (b) Time evolution of total absolute skymion charge density and winding number.

center in a counterclockwise direction, passing through only one type of sublattice. We choose four centers [Fig. 3(a)], each specifying a meron/antimeron and calculate the corresponding winding number over the entire evolution period (Fig. 3). The winding numbers, although initially showing some fluctuating noninteger values originating from the lack of well defined winding centres during the fast and slow relaxation process, eventually attain a steady magnitude of ± 1 for $t \gtrsim 0.6$ ps. Compared to that, the total absolute staggered skymion charge saturates slowly toward a magnitude of two, indicating the presence of four half instantons. It is worth mentioning that the winding number remains unchanged under small changes in the winding center as long as a path encircles it. Therefore, the result remains consistent with the skymionic charge distribution even when the winding center differs from the center of topological charge.

B. Topological structure factor

The evolution of absolute staggered skymion charge and winding numbers ensures the emergence of topological objects with opposite charges coming in pairs, however it does

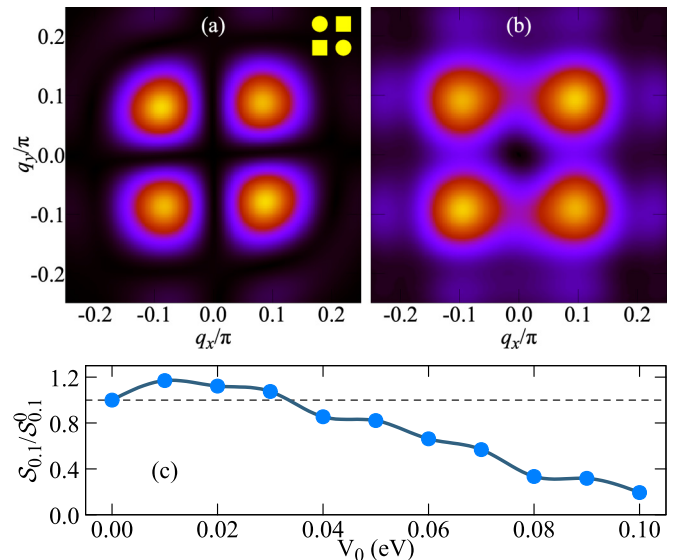


FIG. 4. Topological structure factor and its stability. (a) Topological structure factor of the configuration shown in Fig. 3(a). Inset shows the corresponding real space distribution of the topological charge. (b) Average topological structure factor averaged over 70 different configurations. (c) Average topological structure factor for different strengths of scalar impurity averaged over 32 different configurations and scaled with its average value at $V_0 = 0$. For each configuration we consider the mean value at $q = 0.1(\pm\hat{x} \pm \hat{y})\pi$.

not yet specify the distribution of the topological charge. To determine that we define a topological structure factor

$$S_q = \frac{1}{\mathcal{N}} \sum_{ij} S_{r_i}^s S_{r_j}^s e^{iq \cdot (r_i - r_j)}, \quad (5)$$

where $\mathcal{N} = \sum_i (S_{r_i}^s)^2$ is the normalization constant. One can readily see from Fig. 4(a) that the topological structure factor is reminiscent of a checker-board pattern [Fig. 4(a) inset] which is consistent with the skymionic charge distribution (Fig. 3). However, it is also possible that the laser excited system moves into a spin-spiral configuration or a combination of random clusters with no global long range order. To verify that this is not the case, we consider 70 different configurations with the same normalization constant and evaluate the average distribution of the topological structure factor (Fig. 4). The obtained maxima in the distribution occurs for $q = 0.1(\pm\hat{x} \pm \hat{y})\pi$, which establishes the emergence of a meron-antimeron pair in our 20×20 super cell.

We finally study the robustness of these emergent configurations against disorder. For that, we introduce random onsite energies ranging from $-V_0$ to V_0 , and measure the topological structure factor at points $q = 0.1(\hat{x} \pm \hat{y})\pi$ (Fig. 4). One can readily see that the structure manages to retain its basic features for fairly strong values of the impurity potential, and then gradually collapses into a featureless distribution. Note that a small random impurity can enhance the formation as denoted by the initial rise in average topological structure factor which is consistent with the behavior against small random fluctuations of magnetic moments. This establishes

the robustness of the pair formation process which would be helpful for its physical realization.

IV. CONCLUSIONS

In this work we present a new paradigm for generating nontrivial magnetic textures in antiferromagnets. We show that when excited by an ultrafast laser a two-dimensional antiferromagnet can host meron-antimeron pairs via a thermal Schwinger mechanism. The topological texture can survive for up to 100 ps which makes it possible to observe experimentally. The process is independent of initial helicity of the laser and responsive within a moderate range of frequency and peak amplitude of the laser. We define a staggered skyrmionic charge, winding number, and topological structure factor to demonstrate the formation of topological charge and show that on average the system is more likely to form a pair of meron and antimeron in a checker board pattern. This formation is fairly robust against scalar impurity which makes it easier to observe experimentally. Since the total topological charge of a texture/antitexture pairs is always zero, pairs of different genera can be connected smoothly allowing more flexibility in exploring topological objects of higher genus. Our results thus open a new route to generate out-of-equilibrium topo-

logical features which remain inaccessible in their ground state configuration. This takes us beyond the generation of conventional nontrivial structures such as skyrmions and domain walls, and paves the way to generating more exotic higher-order topological objects such as chiral bobbers [38] or hopfions [39].

ACKNOWLEDGMENTS

We thank Nikolai Kiselev, Stefan Eisebitt, Frank Freimuth, and Olena Gomony for discussions. We acknowledge financial support from Leibniz Collaborative Excellence project OptiSPIN – Optical Control of Nanoscale Spin Textures. We acknowledge funding under SPP 2137 “Skyrmionics” of the DFG and financial support from the European Research Council (ERC) under the European Union’s Horizon 2020 research and innovation program (Grant No. 856538, Project “3D MAGiC”). The work was also supported also by the Deutsche Forschungsgemeinschaft (DFG, German Research Foundation)–TRR 173/2–268565370 (Project A11). We also gratefully acknowledge the Jülich Supercomputing Centre and RWTH Aachen University for providing computational resources.

-
- [1] A. Kirilyuk, A. V. Kimel, and T. Rasing, Ultrafast optical manipulation of magnetic order, *Rev. Mod. Phys.* **82**, 2731 (2010).
- [2] I. Radu, K. Vahaplar, C. Stamm, T. Kachel, N. Pontius, H. A. Dürr, T. A. Ostler, J. Barker, R. F. L. Evans, R. W. Chantrell, A. Tsukamoto, A. Itoh, A. Kirilyuk, T. Rasing, and A. V. Kimel, Transient ferromagnetic-like state mediating ultrafast reversal of antiferromagnetically coupled spins, *Nature (London)* **472**, 205 (2011).
- [3] Y. Yang, R. B. Wilson, J. Gorchon, C.-H. Lambert, S. Salahuddin, and J. Bokor, Ultrafast magnetization reversal by picosecond electrical pulses, *Sci. Adv.* **3**, e1603117 (2017).
- [4] E. Beaupaire, J.-C. Merle, A. Daunois, and J.-Y. Bigot, Ultrafast Spin Dynamics in Ferromagnetic Nickel, *Phys. Rev. Lett.* **76**, 4250 (1996).
- [5] G. P. Zhang and W. Hübner, Laser-Induced Ultrafast Demagnetization in Ferromagnetic Metals, *Phys. Rev. Lett.* **85**, 3025 (2000).
- [6] B. Koopmans, J. J. M. Ruigrok, F. D. Longa, and W. J. M. de Jonge, Unifying Ultrafast Magnetization Dynamics, *Phys. Rev. Lett.* **95**, 267207 (2005).
- [7] B. Koopmans, G. Malinowski, F. Dalla Longa, D. Steiauf, M. Fähnle, T. Roth, M. Cinchetti, and M. Aeschlimann, Explaining the paradoxical diversity of ultrafast laser-induced demagnetization, *Nat. Mater.* **9**, 259 (2010).
- [8] J. K. Dewhurst, P. Elliott, S. Shallcross, E. K. U. Gross, and S. Sharma, Laser-Induced Intersite Spin Transfer, *Nano Lett.* **18**, 1842 (2018).
- [9] F. Willems, C. von Korff Schmising, C. Strüber, D. Schick, D. W. Engel, J. K. Dewhurst, P. Elliott, S. Sharma, and S. Eisebitt, Optical inter-site spin transfer probed by energy and spin-resolved transient absorption spectroscopy, *Nat. Commun.* **11**, 871 (2020).
- [10] J. K. Dewhurst, S. Shallcross, P. Elliott, S. Eisebitt, C. V. K. Schmising, and S. Sharma, Angular momentum redistribution in laser-induced demagnetization, *Phys. Rev. B* **104**, 054438 (2021).
- [11] E. Golias, I. Kumberg, I. Gelen, S. Thakur, J. Gördes, R. Hosseinifar, Q. Guillet, J. K. Dewhurst, S. Sharma, C. Schüßler-Langeheine, N. Pontius, and W. Kuch, Ultrafast Optically Induced Ferromagnetic State in an Elemental Antiferromagnet, *Phys. Rev. Lett.* **126**, 107202 (2021).
- [12] F. Büttner, B. Pfau, M. Böttcher, M. Schneider, G. Mercurio, C. M. Günther, P. Hessian, C. Klose, A. Wittmann, K. Gerlinger, L. M. Kern, C. Strüber, C. von Korff Schmising, J. Fuchs, D. Engel, A. Churikova, S. Huang, D. Suzuki, I. Lemesch, M. Huang, L. Caretta, D. Weder, J. H. Gaida, M. Möller, T. R. Harvey, S. Zayko, K. Bagschik, R. Carley, L. Mercadier, J. Schlappa, A. Yaroslavtsev, L. Le Guyarder, N. Gerasimova, A. Scherz, C. Deiter, R. Gort, D. Hickin, J. Zhu, M. Turcato, D. Lomidze, F. Erdinger, A. Castoldi, S. Maffessanti, M. Porro, A. Samartsev, J. Sinova, C. Ropers, J. H. Mentink, B. Dupé, G. S. D. Beach, and S. Eisebitt, Observation of fluctuation-mediated picosecond nucleation of a topological phase, *Nat. Mater.* **20**, 30 (2021).
- [13] A. Fert, V. Cros, and J. Sampaio, Skyrmions on the track, *Nat. Nanotechnol.* **8**, 152 (2013).
- [14] E. Viñas Boström, A. Rubio, and C. Verdozzi, Microscopic theory of light-induced ultrafast skyrmion excitation in transition metal films, *npj Comput. Mater.* **8**, 62 (2022).
- [15] C. Heo, N. S. Kiselev, A. K. Nandy, S. Blügel, and T. Rasing, Switching of chiral magnetic skyrmions by picosecond magnetic field pulses via transient topological states, *Sci. Rep.* **6**, 27146 (2016).
- [16] A. Ono and S. Ishihara, Photoinduced topological spin texture in a metallic ferromagnet, *J. Phys. Soc. Jpn.* **88**, 023703 (2019).

- [17] S. Ghosh, F. Freimuth, O. Gomonay, S. Blügel, and Y. Mokrousov, Driving spin chirality by electron dynamics in laser-excited antiferromagnets, *Commun. Phys.* **5**, 69 (2022).
- [18] N. Nagaosa and Y. Tokura, Topological properties and dynamics of magnetic skyrmions, *Nat. Nanotechnol.* **8**, 899 (2013).
- [19] J. Preskill, Magnetic Monopoles, *Annu. Rev. Nucl. Part. Sci.* **34**, 461 (1984).
- [20] M. N. Saha, The origin of mass in Neutrons and Protons, *Indian J. Phys.* **10**, 141 (1936).
- [21] O. Gould and A. Rajantie, Magnetic Monopole Mass Bounds from Heavy-Ion Collisions and Neutron Stars, *Phys. Rev. Lett.* **119**, 241601 (2017).
- [22] T. Kobayashi, Monopole-antimonopole pair production in primordial magnetic fields, *Phys. Rev. D* **104**, 043501 (2021).
- [23] N. Gao, S. G. Je, M. Y. Im, J. W. Choi, M. Yang, Q. Li, T. Y. Wang, S. Lee, H. S. Han, K. S. Lee, W. Chao, C. Hwang, J. Li, and Z. Q. Qiu, Creation and annihilation of topological meron pairs in in-plane magnetized films, *Nat. Commun.* **10**, 5603 (2019).
- [24] X. Lu, R. Fei, L. Zhu, and L. Yang, Meron-like topological spin defects in monolayer CrCl₃, *Nat. Commun.* **11**, 4724 (2020).
- [25] M. Augustin, S. Jenkins, R. F. L. Evans, K. S. Novoselov, and E. J. G. Santos, Properties and dynamics of meron topological spin textures in the two-dimensional magnet CrCl₃, *Nat. Commun.* **12**, 185 (2021).
- [26] X. Z. Yu, W. Koshibae, Y. Tokunaga, K. Shibata, Y. Taguchi, N. Nagaosa, and Y. Tokura, Transformation between meron and skyrmion topological spin textures in a chiral magnet, *Nature (London)* **564**, 95 (2018).
- [27] X. Zhang, Y. Zhou, and M. Ezawa, Antiferromagnetic skyrmion: Stability, creation and manipulation, *Sci. Rep.* **6**, 24795 (2016); P. M. Buhl, F. Freimuth, S. Blügel, and Y. Mokrousov, Topological spin Hall effect in antiferromagnetic skyrmions, *Phys. Status Solidi RRL* **11**, 1700007 (2017); B. Göbel, A. Mook, J. Henk, and I. Mertig, Antiferromagnetic skyrmion crystals: Generation, topological Hall, and topological spin Hall effect, *Phys. Rev. B* **96**, 060406 (2017).
- [28] W. Koshibae, N. Furukawa, and N. Nagaosa, Real-Time Quantum Dynamics of Interacting Electrons: Self-Organized Nanoscale Structure in a Spin-Electron Coupled System, *Phys. Rev. Lett.* **103**, 266402 (2009).
- [29] A. Ono and S. Ishihara, Double-Exchange Interaction in Optically Induced Nonequilibrium State: A Conversion from Ferromagnetic to Antiferromagnetic Structure, *Phys. Rev. Lett.* **119**, 207202 (2017).
- [30] M. D. Petrović, B. S. Popescu, U. Bajpai, P. Plecháč, and B. K. Nikolić, Spin and Charge Pumping by a Steady or Pulse-Current-Driven Magnetic Domain Wall: A Self-Consistent Multiscale Time-Dependent Quantum-Classical Hybrid Approach, *Phys. Rev. Appl.* **10**, 054038 (2018).
- [31] J. García-Palacios and F. J. Lázaro, Langevin-dynamics study of the dynamical properties of small magnetic particles, *Phys. Rev. B* **58**, 14937 (1998).
- [32] S. Ghosh and A. Manchon, Nonequilibrium spin density and spin-orbit torque in a three-dimensional topological insulator/antiferromagnet heterostructure, *Phys. Rev. B* **100**, 014412 (2019).
- [33] I. K. Affleck and N. S. Manton, Monopole pair production in a magnetic field, *Nucl. Phys. B* **194**, 38 (1982); I. K. Affleck, O. Alvarez, and N. S. Manton, Pair production at strong coupling in weak external fields, *ibid.* **197**, 509 (1982).
- [34] O. Gould, S. Mangles, A. Rajantie, S. Rose, and C. Xie, Observing thermal Schwinger pair production, *Phys. Rev. A* **99**, 052120 (2019).
- [35] S. Dìgal and A. M. Srivastava, Formation of Topological Defects with Explicit Symmetry Breaking, *Phys. Rev. Lett.* **76**, 583 (1996); E. J. Copeland and P. M. Saffin, Bubble collisions in Abelian gauge theories and the geodesic rule, *Phys. Rev. D* **54**, 6088 (1996); S. Dìgal, S. Sengupta, and A. M. Srivastava, Vortex-antivortex pair production in a first order phase transition, *ibid.* **56**, 2035 (1997).
- [36] T. W. B. Kibble, Topology of cosmic domains and strings, *J. Phys. A: Math. Gen.* **9**, 1387 (1976).
- [37] P. Rybakov, Topological excitations in field theory models of superconductivity and magnetism, Ph.D. thesis (2021) V. M. Kuchkin, B. Barton-Singer, F. N. Rybakov, S. Blügel, B. J. Schroers, and N. S. Kiselev, Magnetic skyrmions, chiral kinks, and holomorphic functions, *Phys. Rev. B* **102**, 144422 (2020).
- [38] F. N. Rybakov, A. B. Borisov, S. Blügel, and N. S. Kiselev, New Type of Stable Particlelike States in Chiral Magnets, *Phys. Rev. Lett.* **115**, 117201 (2015).
- [39] F. N. Rybakov, N. S. Kiselev, A. B. Borisov, L. Döring, C. Melcher, and S. Blügel, Magnetic hopfions in solids, *APL Mater.* **10**, 111113 (2022).